Development of Fault Location Functions in a Real Digital Fault Recorder: Computational Strategies and Validation

Felipe Lopes*, Eduardo Leite Jr.†, Guilherme Zat‡, Allan Scheid†, Moisés David§, Raphael Reis*,
Paulo Godoy‡, Nicolas Pierim‡, Guilherme Justino‡, Jonas Souza‡, Mário Oleskovicz§
* Federal University of Paraiba (UFPB), João Pessoa, Brazil, {felipelopes,raphael.leite}@cear.ufpb.br
† Independent Consulting, Brazil, eduardoleitejr@gmail.com and avs.009@gmail.com
‡ Itaipu Technological Park Foundation, Brazil, {guilherme.zat,paulo.godoy,nicolas.pereira,guilherme.justino}@pti.org.br
§ University of São Paulo, Brazil, {moisesdavi,olesk}@usp.br

***Abstract*—This paper shares experiences acquired during the development of a fault location module (FLM) in a real Digital Fault Recorder and Phasor Measurement (DFRPM) device, which has been designed for the Itaipu utility, Brazil. Hardware and software aspects, as well as computational strategies and innovative solutions used to implement the FLM are addressed. The DFRPM fault location module (DFRPM-FLM) is validated by means of simulations in a Real-Time Digital Simulator, considering fault scenarios in high- and low-inertia systems. The case studies reveal that the adopted computational strategies resulted in a flexible and reliable DFRPM-FLM, which showed to be able to automatically estimate the fault location, without the need for human intervention.**

***Index Terms*—Fault location, phasor-based methods, single-ended fault location, transmission line.**

Acronyms

BJS	Bom Jesus da Lapa Substation
DAQ	Digital Acquisition
DFR	Digital Fault Recorder
DFRPM	Digital Fault Recorder and Phasor Measurement
FL	Fault Location
FLM	Fault Location Module
FPGA	Field Programmable Gate Array
FPTI	Itaipu Technological Park Foundation
GPS	Global Positioning System
IBR	Inverter-Based Resource
IMP	Impedance Method
IRIG	Inter-Range Instrumentation Group
PMU	Phasor Measurement Unit
PPS	Pulse per Second
PTP	Precision Time Protocol
REA	Reactance Method
RTDS	Real-Time Digital Simulator
SEMD	Margem Direita Substation
SEPHFL	Single-Ended Phasor-Based Fault Location
SYS1	Test System 1
SYS2	Test System 2
TBV	Tabocas do Brejo Velho Substation
TKS	Simple Takagi Method
TKN	Negative Sequence Takagi Method
TKZ	Zero Sequence Takagi Method
VHA	Villa Hayes Substation

I. Introduction

Fault location (FL) on transmission lines has been a topic of great interest for utilities worldwide. FL functions estimate the fault point, helping line maintenance crews to act more assertively in the line restoration procedures [1], [2]. Various FL solutions have been proposed over the years, among which manual fault record inspections and automatic calculations using algorithms embedded into line monitoring micro-processed devices stand out [3]–[6]. In cases of manual fault record inspections, a diversity of apps can be used, requiring time and knowledge from the record analyst.

The main issue of the manual fault record analysis comes from the need for rapid system restoration. It leads analysts to work under stressed conditions, increasing the probability of FL errors. In this context, automatic solutions become attractive, at least to obtain preliminary FL estimations, overcoming the need for significant human interventions. In automatic FL schemes, fault distance is calculated by micro-processed devices, being the results often made available in supervisory systems [2]. Thus, human mistakes are avoided, which are critical for disturbance diagnosis procedures [7].

Given the presented context, efforts have been made to develop automatic FL solutions, which are usually embedded into line monitoring devices, such as Digital Fault Recorders (DFRs) and micro-processed relays. Although a great diversity of line monitoring devices can be found in the market, most of them apply classical FL methods, posing difficulties to use alternative FL approaches. To overcome such a limitations, the Itaipu Technological Park Foundation (FPTI-BR) has conducted research activities toward developing its own digital fault recorder and phasor measurement (DFRPM) device, which has been continuously improved over the years. Among the recent improvements, a FL module (FLM) has been implemented. The FLM is based on an innovative combination of two different single-ended multi-method phasor-based FL approaches, such that it switches between different algorithms in order to obtain fault distance estimations as much accurate and reliable as possible [8], [9].

Despite the great experience gained over the years on FL procedures, very few works in the open literature share experiences in developing real FL devices [10], [11]. Even

in the works in which some information can be found, the choices made for the elements used to build the prototypes are usually not discussed, making it difficult to understand the lessons learned from the point of view of the implementation of real FL devices. As a consequence, most researchers and manufacturers share mainly knowledge about FL formulations [12], [13], without much details on practical implementation aspects, neither on software nor hardware levels. Hence, this paper intends to share experiences acquired during the development of the Itaipu's DFRPM fault location module (DFRPM-FLM), including discussions about the adopted computational implementation strategies and auxiliary algorithms. Moreover, hardware configuration choices are justified, the DFRPM historical evolution is explained, and the flow of operations to implement the adopted FL methodology are described. Finally, to validate the DFRPM-FLM, fault studies on high- and low-inertia systems are carried out using a Real-Time Digital Simulator (RTDS). The obtained results reveal a good performance of the DFRPM-FLM, attesting that the development choices have been adequate for the Itaipu needs, resulting in a device able to automatically calculate reliable FL estimations in power grids with different types of generation.

II. Historical Review on the DFRPM Development

The DFRPM has been developed as an initiative of Itaipu Binacional company. Such an utility was born from negotiations between Brazil and Paraguay to explore the hydroelectric potential of the Paraná River, shared by the two countries. Brazil and Paraguay manage the Itaipu Hydro Power Plant, which is the second largest hydroelectric power plant in the world [14]. Besides its generation units, Itaipu also operates some lines which connect their generators to Brazilian and Paraguayan grids, so that FL functions are often required.

The DFRPM project was motivated by the interest of Itaipu Binacional in modernizing DFRs used in its installations. As the DFRPM has been designed by the FPTI, which is an R&D company maintained by Itaipu, continuous investments in researches to improve the device hardware and software have been made. It has allowed Itaipu Binacional to choose functions for DFRPM which can be useful for its own grid, such as phasor measurement, fault recording and, more recently, innovative FL methodologies. Fig. 1 presents a DFRPM unit in operation in the Itaipu Power Plant to monitor a generator interconnection circuit.

The first DFRPM version was designed to be an M-class Phasor Measurement Unit (PMU), following requirements reported in [15]. Such an early DFRPM version will be called hereafter DFRPM-PMU. The first point of attention during the DFRPM-PMU development was the technology to be used for time synchronization, which should meet the IEEE C37.118 requirements [15]. Initially, using separate Global Positioning System (GPS) signal receivers in each DFRPM unit was an option, but it was not adopted due to the need for open-air antennas, which could be a problem for DFRPM units installed into the Itaipu's powerhouse. The second investigated solution consisted in the application of the Inter-Range Instrumentation Group (IRIG) time codes, but it was not considered, because, according to [16], it would require dedicated cables to distribute the time signals, conflicting with the interests of DFRPM developers at that opportunity.

As a third option, the Precision Time Protocol (PTP) was evaluated, which uses the Ethernet network as the communication mean. It showed to be suitable for the DFRPM applications of interest, thus being chosen to provide time synchronization between different DFRPM units. At that opportunity, a market search was carried out to find suppliers of PTP solutions, being the Meinberg products chosen. The grand master clock MRS600 and the slave clock PTP270PEX were adopted in the DFRPM project, because both have the ability to maintain time synchronization without an external reference. Hence, each DFRPM unit has an individual slave clock, providing reference signals of one pulse per second (1 PPS) and local time stamps for DFRPM fault records.

In hardware-based FL solutions, proper digitization and processing of electrical signals are key to assure reliable studies on power grid disturbances. Thus, hardware and software were carefully designed in order to operate as illustrated in the flowchart shown in Fig. 2. In summary, the DFRPM digital acquisition (DAQ) board is equipped with a Field Programmable Gate Array (FPGA), and it receives a 1 PPS signal to generate the data acquisition triggers in both on/off and analog channels (voltages and currents). Once the acquisition clock is configured, the DAQ boards operate

Fig. 1. DFRPM unit in operation in Itaipu Hydroelectric power plant.

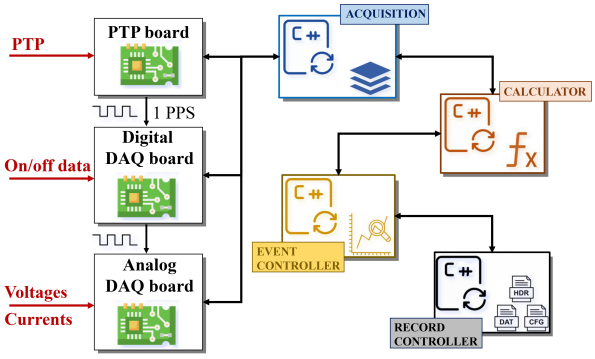

Fig. 2. Flowchart of functionalities embedded into the DFRPM-FLM.

automatically, collecting the field measurements and storing them into internal buffers, whose content is processed via software modules programmed in C++ language. In DFRPM, the number of samples per cycle is configurable in the DAQ boards, such that they can be defined according to the system nominal frequency, i.e., 50 Hz or 60 Hz. For instance, for a 60 Hz system, sampling rates like 64, 128, and 256 samples/cycle can be chosen.

Regarding the data processing strategies, the DFRPM applies different software modules. As shown in Fig. 2, the first module is called "Acquisition" and it collects signal samples and their respective time stamps, buffering them for posterior processing. The stored samples are then processed by a module called "Calculator", which accesses the internal circular buffers as soon as one cycle data is available. Such a module is responsible to apply operations like phasor estimation, total harmonic distortion calculation, power and sequence quantities estimations, among others. Then, results obtained from these operations are used as triggering quantities to activate the record generation, which is managed by the "Event controller" module. Basically, it verifies whether triggering quantities have exceeded predefined thresholds, such that, if so, the "Record controller" module is activated, starting the generation of records in COMTRADE format [17].

The inclusion of FL algorithms in the DFRPM started in 2017, when the DFRPM development crew decided to modernize the early DFRPM-PMU device. The goal was to embed a transmission line single-ended phasor-based FL (SEPHFL) solution, being such a type of function chosen due to two main reasons: 1) because SEPHFL methods require lower data processing capacity in comparison to other solutions, such as traveling wave-based approaches [1]; 2) because communication channels in DFRPM support only the exchange of on/off data, posing difficulties on the implementation of double-ended solutions that would require the analog measurements to be digitized and exchanged between the line terminals. Thus, the data acquisition and communication strategies remained the same of the first DFRPM-PMU version, but due to the need for including new FL functions, a new type of buffer was created. Such a new buffer stores downsampled versions of the already buffered data, reducing the amount of samples to be processed. In the present DFRPM-FLM version, for 60 Hz systems, 16 samples/cycle are analyzed, which is admittedly sufficient for SEPHFL applications.

Since the DFRPM is under continuous improvement, in the near future, data processing and communication functionalities are expected to further evolve, enhancing even more the DFRPM functions and related hardware. However, in this paper, the focus will be maintained on the DFRPM-FLM version, highlighting the FL functions and the computational strategies adopted to implement them. The authors consider that such an experience sharing and the description of innovative SEPHFL solutions (presented in the next sections) consist in the main contributions of this paper. Indeed, besides contributing to the FL area, it fills part of the literature gaps regarding practical methodologies to develop real FL devices.

III. DFRPM-FLM Development Stages

The DFRPM-FLM functions were designed in three stages, which consisted of: 1) Signal processing; 2) Selection of samples; and 3) FL calculations. Fig. 3 depicts a flowchart in which the flow of operations is shown.

Functionalities shown in Fig. 3 were implemented via software considering the processing of samples available into circular buffers when the "Event controller" module identifies a disturbance. Such an implementation strategy was adopted to overcome the need for continuous FLM operation, which would be unnecessary given that FL algorithms are applied only after the transmission line fault is confirmed. It reduces the amount of data processing during normal operation of the monitored system, and allows to implement FL solutions in a simpler manner, since all data related to the event are promptly available prior the FL procedure begins.

The DFRPM development crew also paid great attention to the execution time of the implemented FL functions, because there was the intention to avoid slow calculations. Hence, the FLM was designed as simple as possible, being its functions automatically applied soon after the event recording is complete. By doing so, FL estimations are made available soon after the disturbance takes place, without any need for manual analysis of the fault records. Further details on the functional blocks shown in Fig. 3 are presented next.

A. Signal Processing Stage

As mentioned earlier, the DFRPM-PMU version was programmed to be an M-class PMU, such that long time windows were used to estimate phasors within the accuracy range defined in the C37.118 standard [15]. In [18], real Brazilian fault cases were analyzed to demonstrate that M-class PMU measurements could be used in FL applications, provided that protection and circuit breakers (CBs) with traditional operation times are used. Conventional schemes typically result in fault

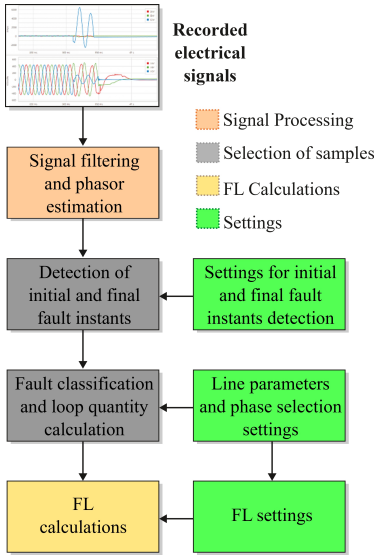

Fig. 3. Flowchart of functionalities embedded into the DFRPM-FLM.

clearance times of about 3 to 5 power cycles, which are sufficient to obtain at least one accurate PMU phasor sample within the fault steady-state period. However, considering the trend to accelerate protections [19], and with the evolving of CB technologies, fault clearance times have been significantly reduced, which can pose difficulties in using M-class PMUs in FL applications [20].

Based on the above-mentioned considerations, among the DFRPM signal processing functionalities, the phasor estimation algorithm was the first one to be reviewed in order to reduce the phasor stabilization time, making it compatible with traditional micro-processed protective relays. The Goertzel algorithm [21], which was already used in the DFRPM-PMU version, was adapted to work with one cycle data window, considering sliding data windows that update their content at each sampling instant. In addition, to overcome eventual filter quality losses due to the data window length reduction, the adaptive DC decaying component removal algorithm reported in [22] was implemented in the DFRPM-FLM. By doing so, phasor stabilization times of one cycle were obtained, with good robustness to the DC decaying component influence.

Fig. 4 shows an example of the phasor calculation during an AG fault in a given line, where $|\hat{I}_{PMU}|$ and $|\hat{I}_{FLM}|$ stand for the magnitude of phasors calculated through the DFRPM-PMU and DFRPM-FLM functions, respectively. The figure assesses only the magnitude of estimated phasors, being enough to evaluate the phasor stabilization times. For didactic reasons, the root mean square values of the calculated phasors are multiplied by $\sqrt{2}$ to match peak values of the analyzed current signal, facilitating the visualization of the phasor transition between pre-fault and fault periods.

The record shown in Fig. 4 regards to a fault cleared in about four cycles, for which both $|\hat{I}_{PMU}|$ and $|\hat{I}_{FLM}|$ presented good response in the presence of the DC decaying component. However, it is noticed that $|\hat{I}_{PMU}|$ only touches the fault steady-state, whereas $|\hat{I}_{FLM}|$ has a faster convergence, resulting in a greater number of samples over the fault steady-state period. Another aspect to be emphasized is that, in $|\hat{I}_{PMU}|$, the reference timestamp is centered in the middle of data window, whereas in $|\hat{I}_{FLM}|$, it is placed in the first window sample. As a result, the perception of the fault beginning instant is different in $|\hat{I}_{PMU}|$ and $|\hat{I}_{FLM}|$. Such a feature would not be a problem for FL applications, as proven in [18], but $|\hat{I}_{FLM}|$ allows to verify signal variations when they indeed begin over the time, facilitating timestamps of fault beginning and ending instants to be managed in the DFRPM-FLM.

Besides the phasor estimation, functions to calculate incremental phasors were also implemented. Incremental phasors are useful for fault studies, since they reproduce the behavior of the pure fault circuit, allowing to estimate fault contributions irrespective of the system loading. To calculate such incremental quantities, pre-fault phasors are subtracted from those measured during the fault period as follows:

$$\Delta\hat{S} = \hat{S} - \hat{S}_{pre} \ , \tag{1}$$

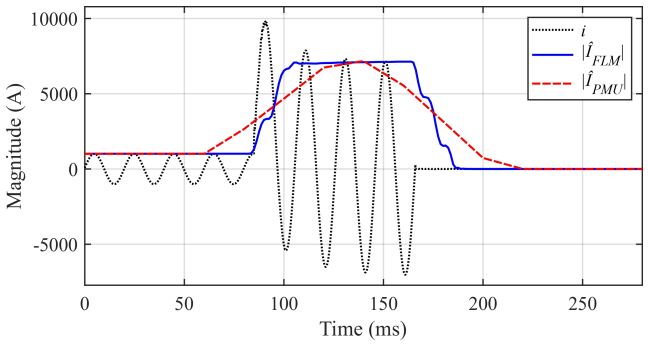

Fig. 4. Comparison between estimated $|\hat{I}_{FLM}|$ and $|\hat{I}_{FLM}|$ phasors.

where $\hat{S}$ is a generic phasor (which can be voltage $\hat{V}$ or current $\hat{I}$), being $\Delta\hat{S}$ and $\hat{S}_{pre}$ the incremental phasor and pre-fault phasor, respectively. In DFRPM-FLM, the pre-fault phasor is taken few samples before the fault beginning instant, which is detected by functions which will be explained later on.

In the DFRPM, the Goertzel phasor estimation method was implemented as a non-recursive algorithm, resulting in time varying phase angles. Thus, it was found that, if pre-fault quantities were taken at a fixed time instant while the reference phasors slide over the time, a problem could occur, because the phase angle reference could change as the time goes by. Hence, an angle correction of estimated phasors is performed in DFRPM-FLM prior the incremental phasor calculation. In summary, phasors are rotated at each sampling instant by an angle $\theta = \frac{2\pi}{N}$, being N the number of samples per cycle in the analyzed data window. Such a procedure is described in [23], being applied in the in DFRPM-FLM as follows:

$$\begin{bmatrix} \hat{S}_{re}(k) \\ \hat{S}_{im}(k) \end{bmatrix} = \begin{bmatrix} \cos(k\theta) & \sin(k\theta) \\ -\sin(k\theta) & \cos(k\theta) \end{bmatrix} \cdot \begin{bmatrix} \hat{S}^{in}_{re}(k) \\ \hat{S}^{in}_{im}(k) \end{bmatrix} \ , \tag{2}$$

where $\hat{S}_{re}(k)$ and $\hat{S}_{im}(k)$ are the k-th sample of the real and imaginary parts of the corrected phasors, respectively, obtained from the analysis of the real and imaginary part of a given input phasor $\hat{S}^{in} = \hat{S}^{in}_{re} + j\hat{S}^{in}_{im}$.

B. Selection of Samples Stage

FL solutions are mathematically valid only during the fault period, such that a valid FL window must be defined in order to encompass stable samples in between the fault inception and the CB electrical opening instant [20]. Thus, according to Fig. 3, the DRPM-FLM selects samples within the referred FL window by applying two procedures, namely: 1) detection of the initial and final instants of the fault; and 2) phase selection procedure. These procedures allow to identify stable samples taken from excited fault loops over the fault steady-state regime. To facilitate the explanations on that, Fig. 5 illustrates the FL window identification procedure implemented in the DFRPM-FLM for a given AG fault case. In the figure, curves are normalized using different bases in order to facilitate the visualization of the depicted variables. Further details on each procedure are presented next.

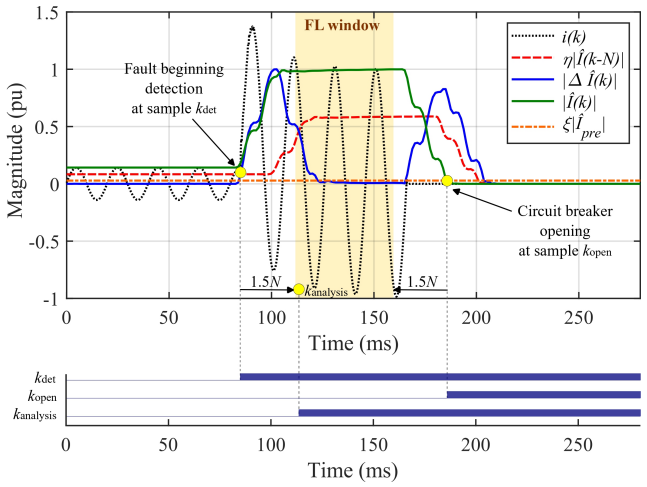

Fig. 5. Example of circuit breaker opening detection using the DFRPM-FLM.

1) Detection of initial and final fault instants: To detect the initial instant of the FL window, magnitudes of positive sequence incremental phasors are compared against a percentage η of past samples of the positive sequence phasors. Thus, the fault beginning sample k_{det} (see Fig. 5) is detected if:

$$|\Delta\hat{S}(k)| > \eta \cdot |\hat{S}(k-N)| \ , \tag{3}$$

otherwise, sample k is incremented and the subsequent samples are processed until the initial fault instant is found. In the present DFRPM-FLM version, $\eta = 0.2$ is considered as a default setting, which was defined after massive simulations.

It is important to mention that the DFRPM-FLM has been developed to be able to properly operate in traditional strong high inertia systems, and in low-inertia weak power grids, such as those with high insertion of inverter-based resources (IBRs). Therefore, the referred disturbance detection procedure was designed to support the analysis of both voltages and currents, being the selection of the reference quantity a DFRPM-FLM user-defined setting. In this context, it is worth mentioning that current- and voltage-based detection procedures have been recommended for strong and weak systems, respectively.

The ending instant of the fault is also required to be identified. Since currents quickly decrease after the electrical opening of CB contacts, the DFRPM-FLM analyzes currents in each phase, comparing them against a percentage ξ of pre-fault currents, such that the CB opening sample k_{open} (see Fig. 5) is detected if:

$$|\hat{I}(k)| > \xi \cdot |\hat{I}_{pre}| \ , \tag{4}$$

otherwise, sample k is incremented and the consecutive samples are analyzed. In DFRPM-FLM, $\xi = 0.2$ was defined as the default setting based on massive simulation studies.

From Fig. 5, it is seen that k_{det} indicates the fault beginning, when phasors are still stabilizing. Furthermore, k_{open} is related to an instant at which phasors already reached values smaller than the threshold ξ. In this context, it is known that using phasors during their convergence periods can result in FL errors, such that non-converged samples must be disregarded. In DFRPM-FLM, $1.5N$ samples are discarded after k_{det} and before k_{open}, respectively (see Fig. 5), properly delimiting the FL window. Regarding that, it is known that faster phasor estimations would enlarge the FL window, since the phasor stabilization periods would be shortened. Even so, shorter windows could worsen the phasor estimation quality, such that a balance between speed and accuracy must exist.

TABLE I
CALCULATION OF LOOP QUANTITIES.

System and fault Type	Selected loop	$\hat{V}_{loop}$	$\hat{I}_{loop}$
Conventional grids and	AG	$\hat{V}_a$	$\hat{I}_a + K_0\hat{I}_0$
systems with IBRs	BG	$\hat{V}_b$	$\hat{I}_b + K_0\hat{I}_0$
(Faults AG, BG, CG)	CG	$\hat{V}_c$	$\hat{I}_c + K_0\hat{I}_0$
Conventional grids	AB	$\hat{V}_a - \hat{V}_b$	$\hat{I}_a - \hat{I}_b$
(AB, BC, CA,	BC	$\hat{V}_b - \hat{V}_c$	$\hat{I}_b - \hat{I}_c$
ABG, BCG, CAG)	CA	$\hat{V}_c - \hat{V}_a$	$\hat{I}_c - \hat{I}_a$
Systems	AB	$\hat{V}_a - \hat{V}_b$	$\hat{I}_a - \hat{I}_b$
with IBRs	BC	$\hat{V}_b - \hat{V}_c$	$\hat{I}_b - \hat{I}_c$
(AB, BC, CA)	CA	$\hat{V}_c - \hat{V}_a$	$\hat{I}_c - \hat{I}_a$
Systems	AB'	$\hat{V}_a + \hat{V}_b$	$\hat{I}_a + \hat{I}_b + 2K_0\hat{I}_0$
with IBRs	BC'	$\hat{V}_b + \hat{V}_c$	$\hat{I}_b + \hat{I}_c + 2K_0\hat{I}_0$
(ABG, BCG, CAG)	CA'	$\hat{V}_c + \hat{V}_a$	$\hat{I}_c + \hat{I}_a + 2K_0\hat{I}_0$

2) Fault Classification and loop quantity calculation: SEPHFL methods are based on the same principles of distance protection elements. Therefore, loop quantities are calculated according to the fault type [1]. In DFRPM-FLM, different phase selection and fault classification techniques have been experimented, including solutions based on sequence components, incremental currents and also on the evaluation of imbalances in the monitored signals [1], [24]. Although these three approaches were embedded into the DFRPM-FLM, the DFRPM developers intend to consider the unbalance-based solution as the default one, since it provides flexibility in using voltages or currents as input signals in strong and weak systems, respectively. Due to space limitations, such a technique is not detailed here, but the authors intend to describe it in future works.

Table I presents the default fault loops implemented in the DFRPM-FLM, which are calculated for single-circuit lines as reported in [1], [25], where $K_0 = \frac{Z_{L0}-Z_{L1}}{Z_{L1}}$ is the zero sequence compensation factor, being Z_{L0} and Z_{L1} the zero and positive sequence line impedances, respectively, and $\hat{I}_0$ the zero sequence current. In summary, classical SEPHFL methodologies classify faults within six loops, which cover short-circuits that excite phase-to-ground (AG, BG, CG) and phase-to-phase (AB, BC, CA) loops. However, for systems with IBRs (which are very weak in nature), the alternative phase-to-phase loops (AB', BC', CA') proposed in [25] for double-phase-to-ground faults have shown to be advantageous, thus being also considered in the DFRPM-FLM project. For applications in double-circuit lines, the loop currents are calculated by adding a zero-sequence coupling compensation factor (as it will be discussed later on), but due to space limitations, only the approach for single-circuit lines is presented here.

As it will be explained in the next section, the DFRPM-FLM analyzes double-phase and double-phase-to-ground faults through different FL formulations. Thereby, fault classification procedures are required rather than only phase selection ones. To do so, the DFRPM-FLM combines the phase selection with a fault grounding connection detection by comparing $\hat{I}_0$ with a pre-defined threshold. As a result, faults can be classified as AG, BG, CG, AB, BC, CA, ABG, BCG, CAG or ABC.

According to Table I, for AG, BG and CG faults, traditional AG, BG and CG loops are selected, respectively, but, if faults involving two phases take place, the loop selection depends on the monitored system type (conventional generation or IBR) and fault type. If the DFRPM-FLM is configured to monitor a conventional grid (strong high-inertia system), loops AB, BC or CA are enabled for AB/ABG, BC/BCG and CA/CAG faults, respectively. On the other hand, if the DFRPM-FLM is set to monitor an IBR-interconnecting line (weak terminal with atypical fault contributions [25]), traditional loops AB, BC and CA are enabled only for AB, BC and CA faults, respectively, being the adapted loops AB', BC' and CA' selected for ABG, BCG and CAG faults, respectively. Such a fault classification procedure is carried out at the first sample of the estimated FL window, called $k_{analysis}$, as highlighted in Fig. 5.

C. FL Calculation Stage

FL calculations start as soon as the fault loop is selected at sample $k_{analysis}$. Only samples stored in the FL window are analyzed, being the remaining ones discarded (see Fig. 5). The SEPHFL solution implemented in the DFRPM-FLM consists in an innovative combination between two different multi-method approaches reported in [8] and [9], which suit for conventional high inertia grids and IBR-interconnecting low inertia systems, respectively. In [8], a fault search field is estimated along with a punctual fault distance estimation. However, here, only the punctual FL calculation is considered, which consists in the median value of the FL estimation samples within the FL window, as proposed in [20].

The complete multi-method SEPHFL methodology developed in the DFRPM-FLM is explained in the flowchart shown in Fig. 6, where single-phase-to-ground faults, double-phase faults, double-phase-to-ground faults and three-phase faults are referred to as PG, PP, PPG and PPP, respectively. As one can see, to calculate the punctual FL estimation, the Reactance Method (REA), Impedance Method (IMP), Simple Takagi Method (TKS), Negative Sequence Takagi Method (TKN) and Zero Sequence Takagi Method (TKZ) are used. In addition, if IBR-interconnecting lines are monitored, the TKZ is modified to apply loops AB', BC' and CA' (see Table I), resulting in the TKZ' method. Furthermore, an additional condition is used to replace the prioritized methods (more complex in nature) by a simpler one, namely, REA, if the prioritized FL estimation indicates a fault out of the line.

Still regarding Fig. 6, it is important to explain that, in PPP fault cases, if IBR-interconnecting lines are considered, a condition related to the IBR control scheme is analyzed. Basically, as recommended in [9], if the IBR control scheme

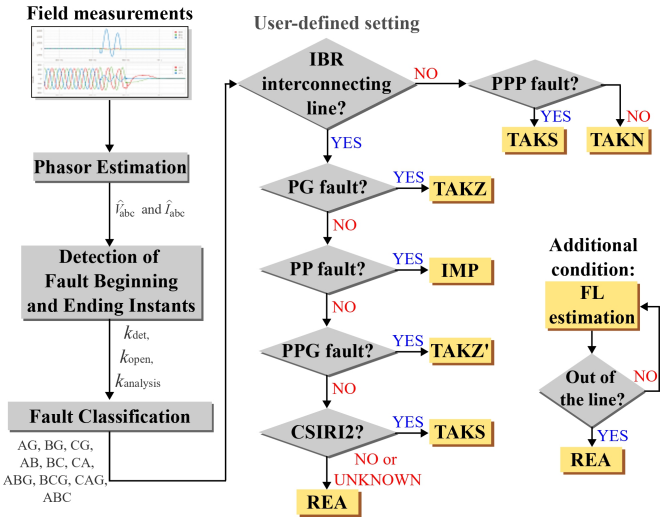

Fig. 6. Flowchart describing the multi-method phasor-based single-ended FL methodology developed in the DFRPM-FLM.

emulates reactive and negative sequence currents (CSIRI2), as proposed in [26], TAKS is used, otherwise REA is applied [9]. Due to space limitations, the mathematical descriptions of the used FL techniques are not presented here, but further details can be found in [1], [8], [9], [12].

IV. DFRPM-FLM Validation

To validate the DFRPM-FLM, RTDS fault simulations were performed using two power system models, called SYS1 and SYS2, whose topologies are shown in Figs. 7 and 8, respectively. SYS1 represents a 500 kV/50 Hz line 348 km long, which connects Margem Direita substation (SEMD) in Brazil to Villa Hayes substation (VHA) in Paraguay. On the other hand, SYS2 consists in a 230 kV/60 Hz line, 149 km long, responsible to connect a photovoltaic power plant at Tabocas do Brejo Velho substation (TBV) to Bom Jesus da Lapa substation (BJS), both located in Brazil. Regarding SYS2, no information on the used IBR control scheme was obtained from the operator, such that the condition CSIRI2 in Fig. 6 was assumed to be unknown. In each system, different fault and system characteristics were considered, varying: fault distance (from 5% to 95% of the line length, with steps of 5%), type (AG, AB, ABT and ABC), inception angle (0 and 90 degrees), resistance (0.01 and 10 Ω) and system loading (light and heavy load scenarios). In both systems SYS1 and SYS2, FL estimations from both line terminals are analyzed, accounting for 2432 FL estimations obtained from the DFRPM-FLM routines.

Fig. 9 presents cumulative polygons of the absolute FL errors ϵ calculated for systems SYS1 and SYS2 when valid FL estimations were obtained. Such polygons show the maximum ϵ values for different percentages of simulated cases, allowing to statistically analyze the DFRPM performance. For the sake of comparison, only TAKS and TAKN methods are assessed, since they are often used in off-the-shelf FL devices. Due to

space limitations, additional comparisons between other particular FL approaches and the implemented one are not presented here. However, further results on comparative studies can be found in [8], [9], where details on the design procedures of the adopted multi-method approaches are reported.

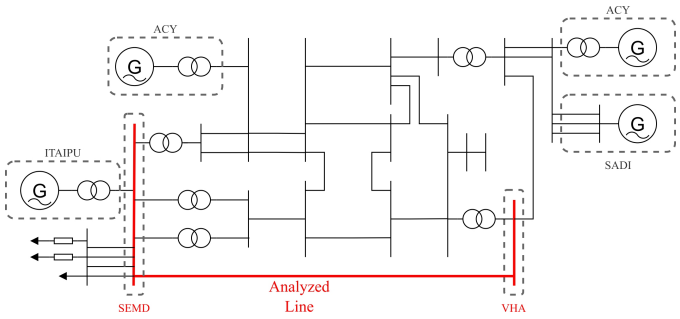

Fig. 7. System 1 (SYS1), consisting of a conventional 500 kV/50 Hz grid.

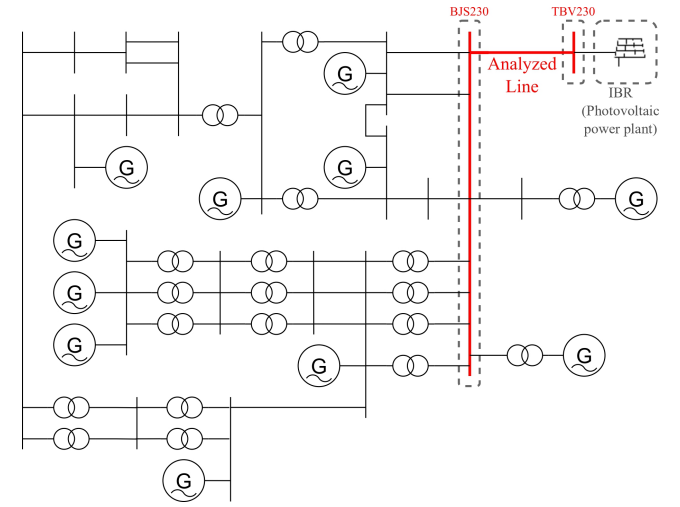

Fig. 8. System 2 (SYS2), consisting of a 230 kV/60 Hz system with IBR.

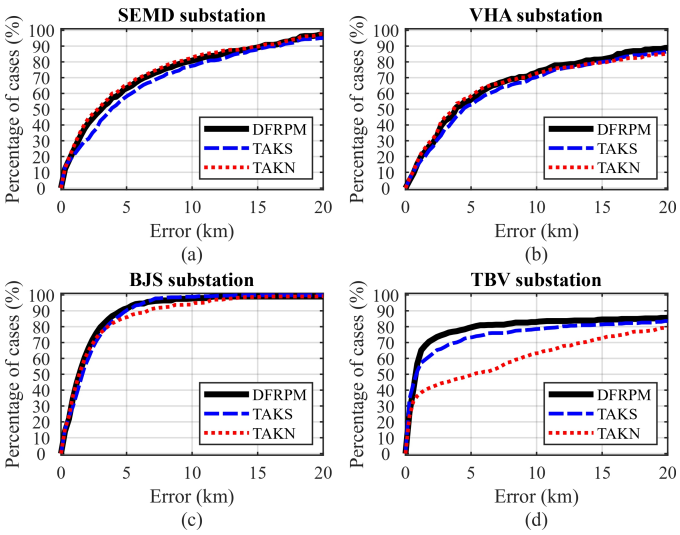

Fig. 9. Cumulative polygon of FL errors at substations: (a) SYS1-SEMD; (b) SYS1-VHA; (c) SYS2-BJS; and (d) SYS2-TBV.

The obtained results reveal that the DFRPM-FLM routines are valid, being capable of automatically calculating reliable FL estimations. For line terminals with conventional generations, as seen in Figs. 9(a), (b) and (c), the DFRPM-FLM performance was very similar to those obtained from TAKS/TAKN methods (very close cumulative polygons), attesting the FLM validity. On the other hand, for weak terminals with IBRs, the DFRPM results showed to be more accurate than those obtained from TAKS/TAKN methods (TAKS/TAKN cumulative polygons are below the DFRPM-FLM one), as depicted in Fig. 9(d). From Figs. 9(a), (b), (c), and (d), it is noticed that ϵ in 80% of the analyzed cases did not exceed 9.6 km, 13.5 km, 3 km and 5.1 km, respectively. These errors represent percentage errors of about 2.8%, 3.9%, 2.0% and 3.4%, respectively, which are within the range expected for SEPHFL methods [27]. If lower percentages of analyzed cases are considered, such as 50% (covering low fault resistance cases), for instance, overall ϵ values smaller than 4 km are verified, attesting the DFRPM-FLM good performance. Thus, one can conclude that the multi-method approaches available in the DFRPM-FLM guarantee reliable FL estimations in both high- and low-inertia grids, thus being promising for FL applications in modern real systems.

V. Additional Remarks and In Progress Activities

In the previous section, the DFRPM was tested for single-circuit transmission lines, demonstrating its performance during FL procedures in lines interconnecting traditional synchronous generations and IBRs. It was sufficient to demonstrate the good performance and the validity of the DFRPM-FLM for FL procedures in high and low inertia systems. However, since this is an ongoing research, there are other important development perspectives that can be shared. Among them, those related to FL applications in double-circuit and series compensated lines stand out.

It is known that most double-circuit lines are transposed in such a way that positive and negative-sequence couplings between the parallel circuits are eliminated. As a result, only a zero-sequence coupling takes place, affecting FL calculations in grounded fault scenarios only. As mentioned earlier, the DFRPM has been programmed to modify the calculation of loop currents to compensate the effects of the referred zero-sequence coupling. To do so, it adds a compensation factor for the mutual coupling between the parallel lines, as recommended in [28], requiring zero-sequence mutual coupling settings and current measurements from the parallel circuit. In relation to the need for additional measurements, it is not a problem for the DFRPM, since it has 32 channels that can be converted into voltage or current inputs.

In addition to the above-mentioned application, series compensated circuits have also been considered in this research. Since sub-synchronous frequencies may originate due to the interaction between the capacitors and system inductances, additional distortions are observed in estimated phasors, challenging FL methods. To minimize these effects, besides using measurements taken from the line side to avoid the influence

of voltages across the series capacitors, using enhanced phasor estimation methods is strongly recommended, and it has been also investigated in this research.

Finally, the authors emphasize that the present version of the DFRPM-FLM can be already applied to double-circuit lines and series compensated lines, but enhanced procedures are expected to be available in the near future, as well as results from the application of the DFRPM-FLM in the field. The in progress research and development activities are mainly focused on the improvement of FL procedures in double-circuit and series compensated lines, but further details on the preliminary results are not shared here due to space limitations. Among the activities in progress, the development of innovative FL methodologies for double-circuit lines and enhanced phasor filtering solutions for series compensated lines stand out, being the results obtained from these new developments expected to be presented in future works.

VI. Conclusions

This paper shared experiences acquired during the development of a real FL device, called DFRPM, presenting information about its hardware, software, and innovative algorithms designed to support FL applications. RTDS massive simulations were carried out to validate the developed device, considering models that represent high- and low-inertia grids.

The obtained results reveal that the computational strategies adopted in the DFRPM design resulted in a reliable device, with promising FL functionalities. Indeed, for both high- and low-inertia power grids, the obtained FL errors showed to be within the range expected for algorithms of the same class, but guaranteeing more accurate results in IBR-interconnecting lines, in which FL procedures by means of traditional techniques tend to be more challenging. These results prove that the DFRPM is promising for real systems, and that the shared experiences on the DFRPM development can be useful for parties interested in developing their own FL schemes.

Acknowledgement

The authors thank the Itaipu Technological Park Foundation (FPTI-BR) for the cooperation and financial support.

References

[1] M. M. Saha, J. J. Izykowski, and E. Rosolowski, *Fault Location on Power Networks*, 1st ed. Springer Publishing Company, Inc., 2009.

[2] B. Kasztenny, "Improving line crew dispatch accuracy when using traveling-wave fault locators," in *46th Annual Western Protective Relay Conference, Spokane, Washington*, 2019, pp. 1–13.

[3] S. L. Zimath, M. A. Ramos, J. S. Filho, J. M. Beck, and N. Mueller, "Traveling wave-based fault location experiences," in *2010 63rd Annual Conference for Protective Relay Engineers*, 2010, pp. 1–7.

[4] A. Guzmán, B. Kasztenny, Y. Tong, and M. V. Mynam, "Accurate and economical traveling-wave fault locating without communications," in *2018 71st Annual Conference for Protective Relay Engineers (CPRE)*, 2018, pp. 1–18.

[5] F. V. Lopes, R. L. A. Reis, and K. M. Silva, "Improving traveling wave-based transmission line fault location by leveraging classical functions available in off-the-shelf devices," *IEEE Transactions on Power Delivery*, vol. 38, no. 4, pp. 2969–2972, 2023.

[6] K. Zimmerman and D. Costello, "Impedance-based fault location experience," in *2006 IEEE Rural Electric Power Conference*, 2006, pp. 1–16.

[7] F. V. Lopes, T. Honorato, R. Reis, and R. Fernandes, "Prevention of human errors in transmission line protection and fault location functions by eliminating the need for settings," in *CIGRE Paris Session*, 2020.

[8] F. V. Lopes, E. J. S. Leite Jr, J. P. G. Ribeiro, A. B. Piardi, A. V. Scheid, G. Zat, and R. G. Espinoza, "Single-ended multi-method phasor-based approach for optimized fault location on transmission lines," *Electric Power Systems Research*, vol. 212, p. 108361, 2022.

[9] M. J. Davi, M. Oleskovicz, and F. V. Lopes, "An impedance-multi-method-based fault location methodology for transmission lines connected to inverter-based resources," *International Journal of Electrical Power & Energy Systems*, vol. 154, p. 109466, 2023.

[10] Z. Zhaobin, Z. Qiran, Y. Qing, Y. Wei, Z. Yongqiang, and C. Tao, "Development of transmission line abnormal warning and fault location device," in *2022 4th International Conference on Electrical Engineering and Control Technologies (CEECT)*, 2022, pp. 246–251.

[11] G. Filatova, A. Petrov, and M. Batmanov, "Research of the algorithm and the prototype device for fault location based on synchronized two-side measurement," in *2020 International Youth Conference on Radio Electronics, Electrical and Power Engineering (REEPE)*, 2020, pp. 1–5.

[12] S. Das, S. Santoso, A. Gaikwad, and M. Patel, "Impedance-based fault location in transmission networks: theory and application," *IEEE Access*, vol. 2, pp. 537–557, 2014.

[13] F. V. Lopes, K. M. Silva, and B. F. Küsel, "Parametric analysis of two-terminal impedance-based fault location methods," in *International Conference on Power Systems Transients*, 2015, pp. 15–18.

[14] J. M. B. Godoy, R. A. de Oliveira, G. Aguayo, E. Rodriguez, A. J. M. Szostak, J. A. d. Santos, A. P. Tochetto, M. L. S. Rios, P. H. Galassi, J. R. Pesente, and R. A. Ramos, "The eccande project: Design, field implementation, and operation of a special protection scheme based on synchronized phasor measurements," *IEEE Transactions on Power Delivery*, vol. 38, no. 3, pp. 1780–1787, 2023.

[15] "Ieee standard for synchrophasors for power systems," *IEEE Std C37.118-2005 (Revision of IEEE Std 1344-1995)*, pp. 1–65, 2006.

[16] M. Han, H. Guo, and P. Crossley, "IEEE 1588 time synchronisation performance for iec 61850 transmission substations," *International Journal of Electrical Power & Energy Systems*, vol. 107, pp. 264–272, 2019.

[17] "Ieee/iec measuring relays and protection equipment – part 24: Common format for transient data exchange (comtrade) for power systems," *IEEE Std C37.111-2013 (IEC 60255-24 Edition 2.0 2013-04)*, pp. 1–73, 2013.

[18] "Real-world case studies on transmission line fault location feasibility by using m-class phasor measurement units," *Electric Power Systems Research*, vol. 196, p. 107261, 2021.

[19] E. O. Schweitzer, B. Kasztenny, A. Guzmán, V. Skendzic, and M. V. Mynam, "Speed of line protection - can we break free of phasor limitations?" in *2015 68th Annual Conference for Protective Relay Engineers*, 2015, pp. 448–461.

[20] F. V. Lopes, E. J. S. Leite, J. P. G. Ribeiro, A. B. Piardi, R. G. Fabián Espinoza, A. V. Scheid, G. Zat, and R. B. Otto, "Phasor-based fault location challenges and solutions for transmission lines equipped with high-speed time-domain protective relays," *Electric Power Systems Research*, vol. 189, p. 106617, 2020.

[21] G. Goertzel, "An algorithm for the evaluation of finite trigonometric series," *American Mathematical Monthly*, vol. 65, p. 34, 1958.

[22] K. M. Silva and B. F. Küsel, "Phasor estimation using a modified sine filter combined with an adaptive mimic filter," in *International Conference on Power Systems Transients*, 2011, pp. 14–17.

[23] K. M. Silva and M. L. S. Almeida, "Positive sequence voltage memory filter for numerical digital relaying applications," *Electronics Letters*, vol. 51, no. 21, pp. 1697–1699, 2015.

[24] T. Adu, "An accurate fault classification technique for power system monitoring devices," *IEEE Transactions on Power Delivery*, vol. 17, no. 3, pp. 684–690, 2002.

[25] A. Hooshyar, M. A. Azzouz, and E. F. El-Saadany, "Distance protection of lines emanating from full-scale converter-interfaced renewable energy power plants—part ii: Solution description and evaluation," *IEEE Transactions on Power Delivery*, vol. 30, no. 4, pp. 1781–1791, 2015.

[26] "IEEE standard for interconnection and interoperability of inverter-based resources (IBRs) interconnecting with associated transmission electric power systems," *IEEE Std 2800-2022*, pp. 1–180, 2022.

[27] "IEEE guide for determining fault location on ac transmission and distribution lines," *IEEE Std C37.114-2014 (Revision of IEEE Std C37.114-2004)*, pp. 1–76, 2015.

[28] G. Ziegler, *Numerical distance protection: principles and applications*. John Wiley & Sons, 2011.